JOURNAL OF GUIDANCE, CONTROL, AND DYNAMICS
Vol. 17, No. 1, January–February 1994

Spinup Dynamics of Axial Dual-Spin Spacecraft

Christopher D. Hall*
Air Force Institute of Technology, Wright-Patterson Air Force Base, Ohio 45433
and
Richard H. Rand†
Cornell University, Ithaca, New York 14853

We consider spinup dynamics of axial dual-spin spacecraft composed of two rigid bodies: an asymmetric platform and an axisymmetric rotor parallel to a principal axis of the platform. The system is free of external torques, and spinup of the rotor is effected by a small constant internal axial torque. The dynamics are described by four first-order differential equations. Conservation of angular momentum and the method of averaging are used to reduce the problem to a single first-order differential equation which is studied numerically. This reduction has a geometric counterpart that we use to simplify the investigation of spinup dynamics. In particular, a resonance condition due to platform asymmetry and associated with an instantaneous separatrix crossing is clearly identified using our approach.

Introduction

A DUAL-SPIN spacecraft consists of two bodies constrained to relative rotation about a shaft connecting the bodies but otherwise free to rotate in space. The bodies are in general flexible and dissipative, as is the connection between them, and all spacecraft are subject to environmental torques such as the gravity gradient torque; however, as a first approximation it is useful to model dual-spin spacecraft as two rigid bodies connected by a rigid shaft and free of external torques. Such a model is made more tractable by further assuming one of the bodies is axisymmetric about the axis of relative rotation. This model is called a gyrostat. The axisymmetric body is called the rotor, or wheel, whereas the other body is called the platform or core body. For the special class of *axial* gyrostats, where the rotor is aligned with a principal axis of the platform, a closed-form solution for the angular momentum in terms of Jacobi's elliptic functions has been given by several authors (see Cochran et al.[1] for further references).

Dual spinners are usually placed into orbit with zero relative angular velocity, then a spinup motor provides an equal and opposite torque to both bodies along the shaft. The effect of the axial torque is to spin up the rotor and despin the platform, thereby transferring all or most of the angular momentum to the rotor. Usually this torque is constant for simplicity of control system design. In practice, this maneuver is complicated by resonances due to asymmetries and imbalances of either or both of the two bodies. Spinup of asymmetric dual-spin satellites has been investigated by Gebman and Mingori,[2] Hubert,[3,4] Junkins and Turner,[5] and Guelman.[6] Gebman and Mingori[2] perturbed from an equilibrium point of the zero axial torque system using matched asymptotic expansions to obtain approximate solutions for the flat spin recovery problem for prolate axial gyrostats with small constant torque. Hubert[3,4] and Junkins and Turner[5] combined quasistatic analyses with simulation to investigate more general gyrostats. Guelman[6] devised an effective control law for attitude recovery from arbitrary initial conditions.

Various related resonance problems have been studied by numerous authors, with important early work by Scher and Farrenkopf,[7] Cochran,[8] and Cochran and Beaty,[9] and more recent studies by Kinsey et al.,[10] Or,[11] and Rand et al.[12] Scher and Farrenkopf[7] were the first to note "resonance traps" due to asymmetry and imbalance. Cochran[8] obtained analytical results identifying cases in which such resonances may exist, and Cochran and Beaty[9] presented additional results regarding these resonances. Kinsey et al.[10] studied spinup resonance due to rotor asymmetry, obtaining an approximate solution for the residual cone angle induced by the passage through resonance. Or[11] investigated resonance due to platform asymmetry and unbalance of either platform or rotor, using linearized equations to determine the effects of varying these parameters. Motivated by analogy with resonance capture in dual-spin spacecraft, Rand et al.[12] used an elliptic function averaging approach similar to that used in the present work to study the dynamics of an eccentric wheel on an elastic support.

In this paper, we perturb from the elliptic function solution for zero axial torque, giving a comprehensive treatment of spinup of asymmetric axial gyrostats where the axisymmetric rotor is parallel to a principal axis of the gyrostat, and spinup is effected by a small constant axial torque. The dynamics are described by four first-order ordinary differential equations, and we use a dimensionless form of the equations, equating the small constant torque to a small parameter ϵ. When $\epsilon = 0$ the system has a closed-form solution in terms of Jacobi's elliptic functions as noted previously. Conservation of angular momentum and the method of averaging are used to obtain a single first-order nonautonomous differential equation, which is valid for small ϵ. This equation involves complete elliptic integrals of the first and third kinds; numerical integration shows that this single equation captures the salient features of spinup dynamics.

The reduction from four differential equations to one has a geometric counterpart which we have found simplifies the framework in which to view spinup dynamics. In contrast to the momentum sphere approach, which requires picturing the gradual evolution of a set of integral curves drawn on a sphere,[3] our approach permits the spinup dynamics to be described by an abbreviated but equivalent flow on a plane.

Equations of Motion

Here we give without derivation the differential equations of motion for the angular momentum variables of a rigid axial gyrostat with zero external torque. Referring to Fig. 1, we

Presented as AAS Paper 91-403 at the AAS/AIAA Astrodynamics Specialist Conference, Durango, CO, Aug. 19–22, 1991; received May 1, 1992; revision received May 7, 1993; accepted for publication May 11, 1993.

*Assistant Professor of Aerospace and Systems Engineering. Member AIAA.

†Professor, Theoretical and Applied Mechanics, 207 Kimball Hall.

denote the platform by $\mathcal{P}$, the rotor by $\mathcal{R}$, and the gyrostat by $\mathcal{P}+\mathcal{R}$. For a derivation, see Hughes.[13]

$$\frac{dh_1}{d\tilde{t}} = \frac{I_2-I_3}{I_2I_3}h_2h_3 \tag{1}$$

$$\frac{dh_2}{d\tilde{t}} = \left(\frac{I_3-I_p}{I_3I_p}h_1 - \frac{h_a}{I_p}\right)h_3 \tag{2}$$

$$\frac{dh_3}{d\tilde{t}} = \left(\frac{I_p-I_2}{I_2I_p}h_1 + \frac{h_a}{I_p}\right)h_2 \tag{3}$$

$$\frac{dh_a}{d\tilde{t}} = g_a \tag{4}$$

where

$\hat{e}_i$ = principal axes of $\mathcal{P}+\mathcal{R}$, $i=1, 2, 3$
g_a = torque applied by $\mathcal{P}$ on $\mathcal{R}$ about $\hat{e}_1$
$h_a = I_s(\omega_s+\omega_1)$, angular momentum of $\mathcal{R}$ about $\hat{e}_1$
$h_i = I_i\omega_i$, angular momentum of $\mathcal{P}+\mathcal{R}$ about $\hat{e}_i$, $i=2, 3$
$h_1 = I_1\omega_1 + I_s\omega_s$, angular momentum of $\mathcal{P}+\mathcal{R}$ about $\hat{e}_1$
I_i = moment of inertia of $\mathcal{P}+\mathcal{R}$ about $\hat{e}_i$, $i=1, 2, 3$
$I_p = I_1 - I_s$, moment of inertia of $\mathcal{P}$ about $\hat{e}_1$
I_s = moment of inertia of $\mathcal{R}$ about $\hat{e}_1$
$\tilde{t}$ = time
ω_i = angular velocity of $\mathcal{P}$ about $\hat{e}_i$, $i=1, 2, 3$
ω_s = angular velocity of $\mathcal{R}$ about $\hat{e}_1$ relative to $\mathcal{P}$

Since there are no external moments, angular momentum is conserved and a first integral of the motion is

$$h^2 = h_1^2 + h_2^2 + h_3^2 = \text{const} \tag{5}$$

This integral can be used to reduce the number of equations by one. Furthermore, if $g_a = 0$, there are two additional first integrals which are used to obtain the elliptic function solution. Before proceeding, we simplify notation by changing to dimensionless variables.

Dimensionless Equations

The transformation of Eqs. (1-4) to dimensionless form is obtained by scaling the four momenta, time, and axial torque as follows[6]:

$$x_1 = h_1/h \qquad \mu = h_a/h$$
$$x_2 = h_2/h \qquad t = h\tilde{t}/I_p \tag{6}$$
$$x_3 = h_3/h \qquad \epsilon = g_aI_p/h^2$$

Derivatives with respect to t are denoted by an overdot: $(\dot{}) = d(\ )/dt$. Furthermore, we define three dimensionless inertia parameters by

$$i_j = 1 - I_p/I_j, \qquad j = 1, 2, 3 \tag{7}$$

Carrying out this change of variables leads to the equivalent set of dimensionless equations:

$$\dot{x}_1 = (i_2-i_3)x_2x_3 \tag{8}$$

$$\dot{x}_2 = (i_3x_1-\mu)x_3 \tag{9}$$

$$\dot{x}_3 = -(i_2x_1-\mu)x_2 \tag{10}$$

$$\dot{\mu} = \epsilon \tag{11}$$

Note that we have assumed $h \neq 0$. The $h = 0$ case is called the zero momentum gyrostat[13] and is not considered further here.

Finally, we note that the angular momentum integral, Eq. (5), becomes

$$x_1^2 + x_2^2 + x_3^2 = 1 \tag{12}$$

which defines a unit sphere in R^3, called the momentum sphere.

Inertia Parameters

Of the three inertia parameters defined by Eq. (7), only i_2 and i_3 appear in Eqs. (8-11). These parameters define the shape of the spacecraft, and we adopt the following nomenclature to describe the possibilities: An axial gyrostat is oblate if $I_p > I_2 > I_3$, or, equivalently, if $i_3 < i_2 < 0$; it is prolate if $I_2 > I_3 > I_p$, or if $i_2 > i_3 > 0$; and it is intermediate if $I_2 > I_p > I_3$, or if $i_3 < 0 < i_2$. The body axes have been chosen so that $I_2 > I_3$.

The other inertia parameter, i_1, simplifies to $i_1 = I_s/\bar{I}_1$, the ratio of the axial moment of inertia of $\mathcal{R}$ to the axial inertia of $\mathcal{P}+\mathcal{R}$. Thus, $0 < i_1 < 1$, with the limiting cases $i_1 = 0$ and $i_1 = 1$ corresponding to spacecraft with rod-shaped rotor and rod-shaped platform, respectively. Note that the definitions for oblate, prolate, and intermediate used here do not involve i_1. Thus a spacecraft with major axis $\hat{e}_1$, i.e., $i_1 > i_2 > i_3$, may be either oblate, prolate, or intermediate. Since i_1 does not appear in Eqs. (8-11), the dynamics are independent of the inertia

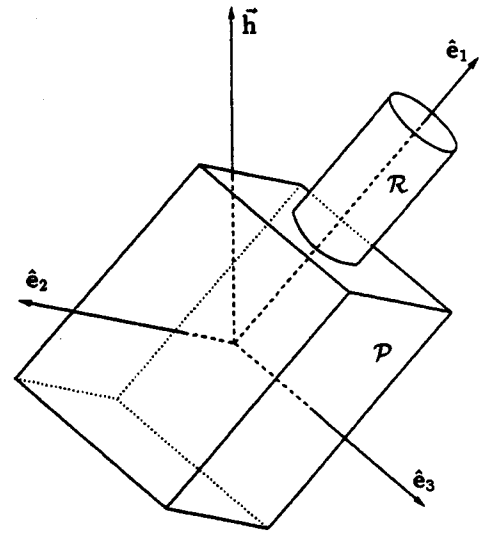

Fig. 1 Gyrostat model of axial dual-spin spacecraft.

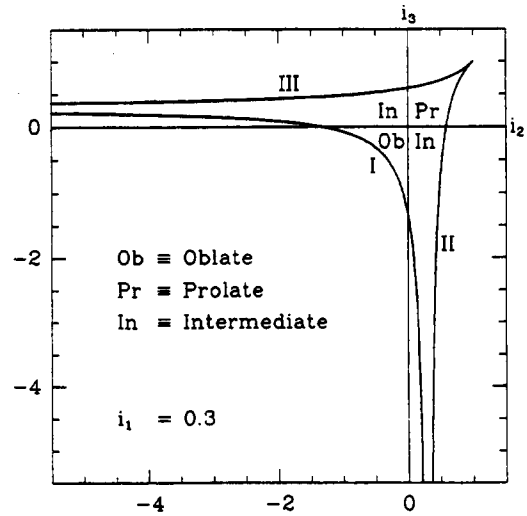

Fig. 2 Admissible inertia parameters [cf. Eq. (13)].

ratio $I_s/I_1 = i_1$. The importance of i_1 is in determining initial conditions for specific cases. In particular, one can show that the all-spun condition ($\omega_s = 0$) corresponds to $\mu = i_1 x_1$.

Another role for i_1 is in limiting physically possible values of i_2 and i_3 using the triangle inequalities for moments of inertia.[13] We have already noted that $0 < i_1 < 1$, and applying the triangle inequalities to i_2 and i_3 restricts physically possible values of these parameters to a specific region of the $i_2 i_3$ plane depending on the value of i_1 as shown in Fig. 2. The boundary curves in Fig. 2 are given by

$$i_3 = \begin{cases} (1 - 2i_1 + i_1 i_2)/(i_2 - i_1) & \text{I} \\ (2i_2 - i_1 i_2 - 1)/(i_2 - i_1) & \text{II} \\ (1 - i_1 i_2)/(2 - i_1 - i_2) & \text{III} \end{cases} \tag{13}$$

where the Roman numerals correspond to the labels in the figure. Note that i_2 and i_3 are both less than 1 for prolate gyrostats, whereas they are unbounded for intermediate gyrostats. The boundary curve I limits i_2 and i_3 for oblate gyrostats.

It is shown in Ref. 14 that the equations of motion are equivalent for oblate and prolate gyrostats. In the present notation, Eqs. (8–11) are unchanged when $(x_1, x_2, x_3, i_2, i_3)$ are replaced by $(-x_1, x_3, -x_2, -i_3, -i_2)$. Herein we only treat oblate gyrostats, with prolate gyrostats implicit by this symmetry transformation. Equivalent results for intermediate gyrostats are given in Refs. 15 and 16.

Reduction of Order

In case there is no axial torque ($\epsilon = 0$), we can reduce the four equations, Eqs. (8–11), to a single elliptic integral. Even when $\epsilon \neq 0$, conservation of angular momentum means we can reduce the number of equations from four to three. In this section we carry out these reductions, beginning with the reduction to quadrature for $\epsilon = 0$.

It is well known[13] that for $\epsilon = 0$ there are three integrals of the motion, namely, kinetic energy, angular momentum, and axial angular momentum of the rotor. Of these three integrals, only total angular momentum is conserved for $\epsilon \neq 0$; the other two quantities are slowly varying for small ϵ, and our approach is to use these slow variables instead of the transverse components of the angular momentum, x_2 and x_3. Kinetic energy is not, however, the most convenient quantity to use, so we choose an equivalent quantity which is a combination of kinetic energy, angular momentum, and rotor angular momentum.

The dimensionless rotational kinetic energy is given by

$$T = \left[(x_1 - \mu)^2 + (1 - i_2)x_2^2 + (1 - i_3)x_3^2 + (1 - i_1)\mu^2/i_1\right]/2 \tag{14}$$

When $\epsilon \neq 0$, the kinetic energy varies according to

$$\dot{T} = \epsilon(-x_1 + \mu/i_1) \tag{15}$$

By subtracting $(\mu^2/i_1 + x_1^2 + x_2^2 + x_3^2)$ from $2T$, and making use of Eq. (12), we obtain a new first integral of the unperturbed system

$$y \triangleq 2T - \mu^2/i_1 - 1 = -2\mu x_1 - i_2 x_2^2 - i_3 x_3^2 \tag{16}$$

whose time derivative for $\epsilon \neq 0$ is

$$\dot{y} = -2\epsilon x_1 \tag{17}$$

We refer to y as the energy. Our motivation for defining y is primarily that $\dot{y}$ is a simpler expression than $\dot{T}$, and we use this fact subsequently. However, the form of y also allows us to write the transverse angular momenta as

$$x_2^2(x_1; \mu, y) = \left[y_2(x_1; \mu) - y\right]/(i_2 - i_3) \tag{18}$$

$$x_3^2(x_1; \mu, y) = \left[y - y_3(x_1; \mu)\right]/(i_2 - i_3) \tag{19}$$

where

$$y_2(x_1; \mu) = i_3 x_1^2 - 2\mu x_1 - i_3 \tag{20}$$

$$y_3(x_1; \mu) = i_2 x_1^2 - 2\mu x_1 - i_2 \tag{21}$$

Note that since $i_2 > i_3$, and since x_2 and x_3 are real, Eqs. (18) and (19) imply that $y_3(x_1; \mu) \leq y \leq y_2(x_1; \mu)$, hence admissible values of the energy y are bounded by these parabolas in the $x_1 y$ plane. Substituting Eqs. (18) and (19) into Eq. (8) gives

$$\dot{x}_1 = \pm\sqrt{y_2(x_1; \mu) - y}\,\sqrt{y - y_3(x_1; \mu)} \tag{22}$$

Since μ and y are constants for $\epsilon = 0$, this equation is separable, and in a later section we give the solution in terms of elliptic functions.

In case $\epsilon \neq 0$, neither μ nor y is constant and the system is evidently nonintegrable. However, we can reduce the number of equations from four to three. Equation (22) for $\dot{x}_1$ is still valid, with the additional caveat that y and μ depend on time, so that the equation is not separable. Thus $\dot{x}_1$, $\dot{y}$, and $\dot{\mu}$ are free of x_2 and x_3. Having eliminated x_2 and x_3, from now on we drop the subscript on x_1. Thus we reduce the four differential equations (8–11) to three:

$$\dot{x} = \pm\sqrt{y_2(x, \mu) - y}\,\sqrt{y - y_3(x, \mu)} \tag{23}$$

$$\dot{y} = -2\epsilon x \tag{24}$$

$$\dot{\mu} = \epsilon \tag{25}$$

where $y_2(x, \mu)$ and $y_3(x, \mu)$ are defined by Eqs. (20) and (21).

This set of equations is equivalent to the original system, even though these are more difficult to integrate numerically due to the bookkeeping involved in keeping track of which branch a trajectory is currently on. The significance of these equations is that they separate the motion into the "fast" oscillations of x and the "slow" variation of y and μ. Integration of Eq. (25) gives $\mu = \epsilon t$ plus a constant of integration. Thus μ may be regarded as the slow time. Later we will see that the slow variation of y vs μ captures most of the dynamics of the system.

Graphical Representations

There are several ways to depict graphically the dynamics of gyrostats. We begin with a brief discussion of the $\epsilon = 0$ dynamics, then discuss the $\epsilon \neq 0$ case. As noted previously, we only treat oblate gyrostats, with prolate gyrostats implicitly included by a symmetry transformation. See Refs. 15 and 16 for equivalent results for intermediate gyrostats.

As was shown in the previous section, when $\epsilon = 0$ the motion is essentially one dimensional [Eq. (22)]. Since the motion is confined to the surface of the momentum sphere, trajectories are one-dimensional constant energy curves on the sphere. The topology of the phase space on the sphere depends on the constant value of μ, as shown in the left half of Fig. 3. For fixed μ, there is a range of possible y values, with each integral curve corresponding to a constant value of y; and there are either two, four, or six equilibrium points on the sphere. The point at the north pole of the sphere, $(x_1, x_2, x_3) = (1, 0, 0)$, is an equilibrium point for all values of μ and is the point at which an oblate dual-spinner typically operates. The notation O_μ denotes this equilibrium point, with the subscript μ indicating that the dynamics depend on the value of μ. For example, O_1 denotes the north pole of the momentum sphere for $\mu = 1$. Similarly, with the symmetry transformation of Ref. 14, the equilibrium at the south pole is associated with the operating condition of a prolate spacecraft, hence the notation P_μ.

The saddle points correspond roughly to unstable transverse spin motions and are denoted by U_μ. Note that these equilibria

do not exist in the lower two spheres in Fig. 3; at $\mu = -i_2$, the two saddles U_μ coalesce with the center P_μ in a pitchfork bifurcation,[17] creating a saddle at the south pole. This value of μ is identified by the symbol μ_2. The equilibria in the "eyes" of the saddle connections correspond roughly to transverse spin about the $\hat{e}_3$ axis and are denoted by T_μ. At $\mu = -i_3$, these centers coalesce with the saddle at the south pole in another pitchfork bifurcation, creating a center there. We denote this bifurcation value of μ by μ_3.

We now introduce the xy plane which we relate directly to the momentum sphere. Using Eqs. (20) and (21) we have plotted $y_2 = y_2(x; \mu)$ and $y_3 = y_3(x; \mu)$ in the right half of Fig. 3 using the same values of μ, i_2, and i_3 as for the spheres. Recall that $y_3 \le y \le y_2$, so the motion is confined to the closed region between the two parabolas. The parabolas intersect at $x = \pm 1$, with $y_2(+1; \mu) = y_3(+1; \mu) = -2\mu$, and $y_2(-1; \mu) = y_3(-1; \mu) = +2\mu$. This is expected since $x = \pm 1$ are equilibrium points (O_μ and P_μ) for all μ, and these intersections correspond to those equilibria. This also implies that the energy at O_μ is -2μ, whereas the energy at P_μ is $+2\mu$.

The extrema of the two parabolas are $y_2(\mu/i_3; \mu) = -(\mu^2/i_3 + i_3)$ and $y_3(\mu/i_2; \mu) = -(\mu^2/i_2 + i_2)$ and are maxima for oblate gyrostats. The maximum of y_2 corresponds to the two centers T_μ, whereas the maximum of y_3 corresponds to the two saddles U_μ. The dashed line passing through the maximum of y_3 for $\mu < \mu_2 = -i_2$ represents the separatrices of the two saddles U_μ. The dashed line $y = 2\mu$ for $\mu_2 < \mu < \mu_3$ represents the separatrices of the saddle P_μ.

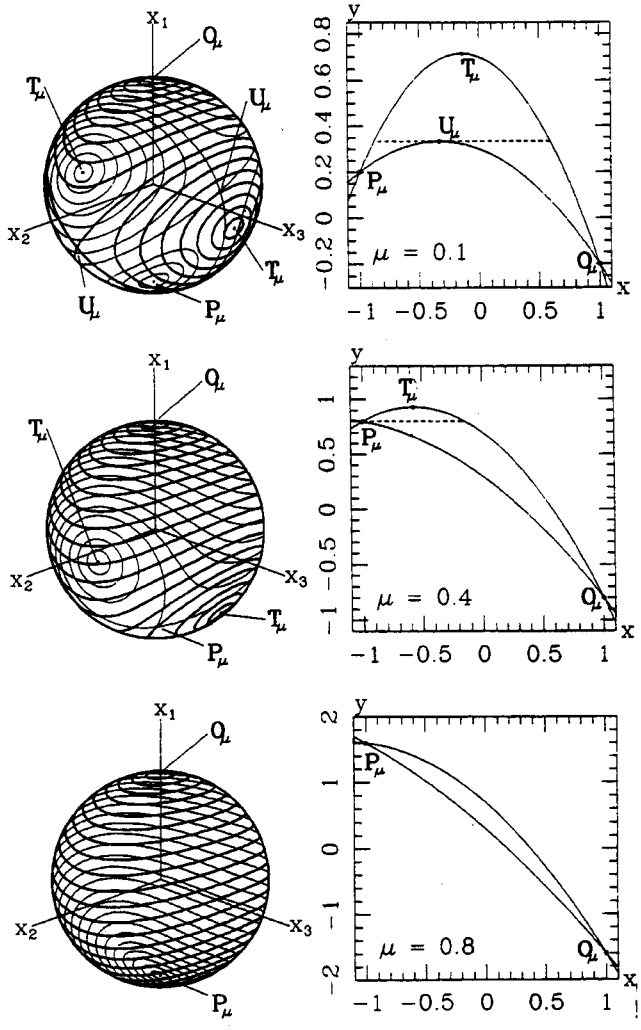

Fig. 3 Momentum spheres and xy plane ($i_2 = -0.3$, $i_3 = -0.7$, $\mu = \{0.1, 0.4, 0.8\}$).

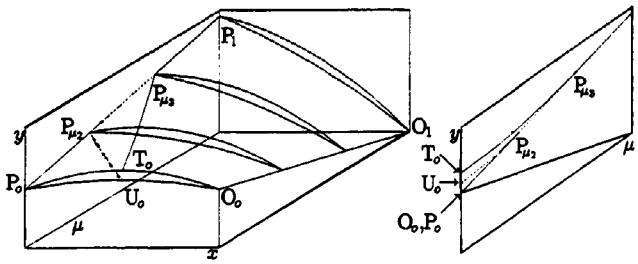

Fig. 4 The $x\mu y$ phase space and μy plane.

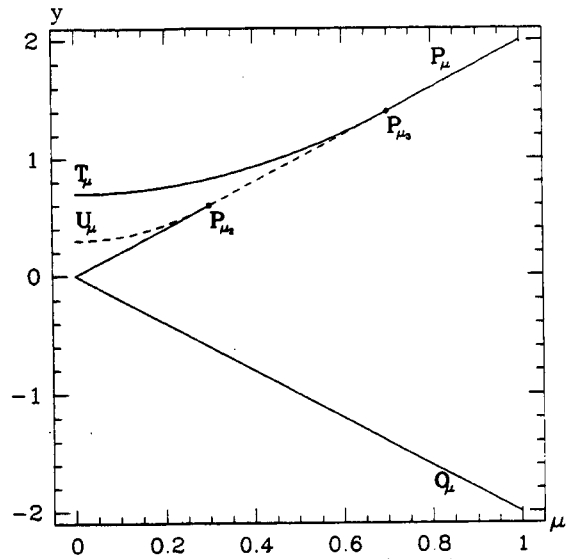

Fig. 5 The μy plane ($i_2 = -0.3$, $i_3 = -0.7$).

In analogy with the momentum spheres, fixing μ fixes the parabolas y_2 and y_3, giving a specific region in the xy plane, and fixing y defines a particular one-dimensional path which $x(t)$ must follow, i.e., the straight line $y = \text{const}$. The equilibrium points in the xy plane are labeled using the same notation as used for the spheres.

When $\epsilon \neq 0$ the dynamics on the momentum sphere become more complicated. In particular, the transverse (T_μ) and saddle (U_μ) equilibria are no longer fixed points of the governing equations; however, O_μ and P_μ are equilibria. Furthermore, when $\epsilon = 0$ the saddle connections are true separatrices, separating qualitatively different motions, but for $\epsilon \neq 0$, trajectories can cross the "instantaneous" separatrices.[18] An instantaneous separatrix crossing occurs when a trajectory of the perturbed ($\epsilon \neq 0$) system crosses a separatrix of the unperturbed ($\epsilon = 0$) system. Although one could generate a sequence of instantaneous spheres valid for fixed values of μ, the path followed by a particular initial condition would be unknown.

Our approach is to construct a sequence of instantaneous xy planes for fixed values of μ, then project the critical points of the instantaneous y_2 and y_3 curves onto the μy plane. This is done in Fig. 4, with a view of the μy plane given in Fig. 5. Solid curves in the μy plane represent centers on the momentum sphere, whereas dashed curves represent saddles and their separatrices.

The μy plane is a simple graphical device for depicting spinup dynamics of axial dual-spin spacecraft. When compared with the momentum sphere approach, the μy plane has the advantage of only requiring one figure to show an entire spinup trajectory, as we illustrate in the next section. In the remainder of this paper, we prove the general validity of projecting the solutions of the original fourth-order system onto this two-dimensional figure. As will be shown, for small

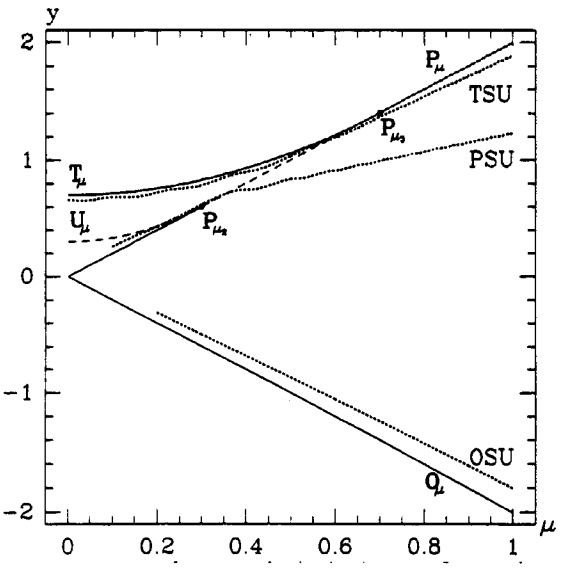

Fig. 6 The μy plane with spinup trajectories ($i_2 = -0.3$, $i_3 = -0.7$).

spinup torques, an initial condition in the μy plane has an approximately unique solution in the plane as long as no instantaneous separatrix crossings occur.

The μy plane is useful not only as the slow state space, but also as a bifurcation diagram for investigating $\epsilon = 0$ dynamics. For $\epsilon = 0$, a given point in the μy plane corresponds to a specific constant energy curve ($y = \text{const}$) on a specific momentum sphere ($\mu = \text{const}$). The missing information is the phase or location of a point on the constant energy curve. Note that the μy plane is symmetric about $\mu = 0$, since the equations of motion are unchanged when (x, μ, t) are replaced by $(-x, -\mu, -t)$; thus we only need to consider $\mu \geq 0$. Also, for $\mu > \mu_3$, there are no additional bifurcations: the momentum spheres, the xy planes, and the μy plane remain qualitatively the same.

Spinup Problems

A spinup maneuver for a dual-spin satellite typically begins with the vehicle operating near a stable equilibrium point, i.e., near O_μ, P_μ, or T_μ, depending on the type of spacecraft. The initial condition also usually corresponds to an all-spun condition, with rotor and platform spinning as a single rigid body with no relative rotation, in which case $\mu = i_1 x_1$. The spinup torque ϵ is then used to increase the rotor momentum μ to the desired operating value, typically near $\mu = 1$, after which the motor is turned off. An energy dissipation mechanism then reduces the final cone angle to zero by damping the transverse momentum ($x_2 = x_3 = 0$). To obtain an inertially fixed platform ($\omega_1 = 0$), it is necessary to spin up the rotor until $\mu = 1$. To see this, refer to the original variables, where $h_2 = h_3 = 0$ implies $\omega_1 = (h - h_a)/I_p = (1 - \mu)/(I_p/h)$. Hence, $\omega_1 = 0$ implies $\mu = 1$. Thus we restrict our attention to the interval $0 \leq \mu \leq 1$.

Referring to Fig. 6, we define three kinds of spinup problems, based on which type of equilibrium the initial condition is near. The flow, i.e., solutions to Eqs. (8-11), for each of the three spinup problems is shown projected onto the μy plane. The energy y is calculated using Eq. (16), after numerically integrating Eqs. (8-11).

Oblate spinup (OSU) starts near O_μ, in the all-spun state, with $x \approx 1$, $\mu \approx i_1$, and $y \approx -2i_1$. As may be seen in Fig. 6, the oblate spinup trajectory in the μy plane is nearly a straight line, and does not cross either of the dashed lines representing the separatrices.

Prolate spinup (PSU) starts near the south pole, or P_μ, with $x \approx 1$, $\mu \approx i_1$, and $y \approx 2i_1$. Unlike the oblate case, however, the y vs μ trajectory is not nearly a straight line. Near $\mu = \mu_2$, the trajectory crosses two instantaneous separatrices. These crossings account for the sharp bend in the path shown in Fig. 6, with the physical interpretation of a large increase in the cone angle.

Transverse spinup (TSU) begins with the vehicle spinning about the $\hat{e}_3$ axis, with $x \approx 0$, $x_3 \approx \pm 1$, $\mu \approx 0$, and $y \approx -i_3$. This type of trajectory includes both flat spin recovery, which was investigated in Ref. 2 for the specific initial condition $x_3 = 1$, $\mu = 0$, and the dual-spin turn described in Ref. 3. As shown in Fig. 6, the trajectory follows the locus of T_μ equilibria, then crosses the dashed line which represents the locus of saddles at the south pole and their separatrices.

Whereas our definitions of the three types of spinup problems are based on the initial conditions, it is also possible to categorize the three cases by the number of instantaneous separatrix crossings that occur. Oblate spinup trajectories cross no separatrices, whereas transverse spinup trajectories cross one instantaneous separatrix and prolate spinup trajectories cross two.

At this point a remark is in order regarding the effect of the magnitude of the spinup torque ϵ on the nutation or cone angle at the conclusion of spinup. The final values of y and μ for a particular trajectory may be used directly to compute an average residual nutation angle as will be seen presently. The closer the final point is to P_μ (for prolate spacecraft) or O_μ (for oblate spacecraft), the smaller the cone angle. Note that in Fig. 6, the final cone angle for prolate spinup is greater than for transverse spinup. This illustrates an important difference between these two types of trajectories: For transverse spinup, making the torque smaller generally decreases the residual cone angle, whereas for prolate spinup smaller torque generally increases the cone angle. Therefore, for transverse spinup, the small torque assumption is relevant in a practical sense. For prolate spinup, however, one would expect a large torque to be used to obtain a smaller final cone angle.

$\epsilon = 0$ Solution

The closed-form solution to Eq. (22) depends on the roots of the quartic polynomial in x

$$[y_2(x;\mu) - y][y - y_3(x;\mu)] = 0 \tag{26}$$

where $y_2(x;\mu)$ and $y_3(x;\mu)$ are quadratics given in Eqs. (20) and (21). The roots in turn depend on the constant values of μ and y, as well as on the parameters i_2 and i_3. Since the solution is well known,[1] we only give the form of the solution here. For further details, see Refs. 15 and 16. The integral tables in Ref. 19 were used extensively in developing the solutions given here and in the next section.

When the roots of Eq. (26) are real, the $\epsilon = 0$ solution is

$$x(u;k) = \beta\left\{\frac{1 - \alpha_1^2 \mathrm{sn}^2(u;k)}{1 - \alpha^2 \mathrm{sn}^2(u;k)}\right\} \tag{27}$$

where $u = \lambda t + u_0$ and the parameters β, α^2, α_1^2, λ, and k depend only on the roots. When two of the roots of Eq. (26) are complex, the solution has the form

$$x(u;k) = \beta\left\{\frac{1 + \alpha_1 \mathrm{cn}(u;k)}{1 + \alpha \mathrm{cn}(u;k)}\right\} \tag{28}$$

where again $\mu = \lambda t + u_0$ and the parameters β, α^2, α_1^2, λ, and k depend only on the roots.

In the elliptic function solutions just given, $\mathrm{sn}(u;k)$ and $\mathrm{cn}(u;k)$ are the sine amplitude and cosine amplitude, respectively; u is the argument or phase, and k is the modulus. It can be shown that on the solid curves in the μy plane, $k = 0$, whereas on the dashed curves, $k = 1$. These functions are periodic in u, with period $4K(k)$, where $K(k)$ is the complete elliptic integral of the first kind, with $K(0) = \pi/2$, and $K(1) = \infty$.

Table 1 Representative relative error (%) of averaged solution vs exact solution

Spinup problem	ϵ 0.0001	0.001	0.01	0.1	1.0
OSU	0.000033953	0.00025270	0.0017994	0.078469	1.3351
TSU	0.0037780	0.49726	3.8177	[a]	[a]
PSU	2.8468	18.471	[a]	[a]	[a]

[a] % error > 50%.

Averaging

Recall that the equations $\dot{y} = -2\epsilon x$ and $\dot{\mu} = \epsilon$ represent the slow flow of the system, whereas Eq. (23) for $\dot{x}$ describes the fast dynamics. The slow equations are in the correct form for averaging,[20] and solutions to the averaged equations remain within $\mathcal{O}(\epsilon)$ of solutions to the unaveraged equations on a time scale of $\mathcal{O}(1/\epsilon)$. Although the method of averaging can be extended to higher order to obtain more accurate approximate solutions on an $\mathcal{O}(1/\epsilon)$ time scale, we demonstrate subsequently that first-order averaging is accurate as long as trajectories do not cross the instantaneous separatrices of the unperturbed system. Furthermore, higher order averaging will not alleviate the separatrix crossing problem, for reasons discussed in the following section.

We form the averaged equations by replacing the right-hand sides of $\dot{y}$ and $\dot{\mu}$ by their averages over one period of the $\epsilon = 0$ solution for x

$$\dot{\bar{y}} = -2\epsilon\bar{x} \tag{29}$$

$$\dot{\mu} = \epsilon \tag{30}$$

where $\bar{x} = \bar{x}(y, \mu)$ is defined by

$$\bar{x} = \frac{1}{4K}\int_0^{4K} x(u; k)\, du \tag{31}$$

depends on the form of the $\epsilon = 0$ solution, and $\bar{y}$ is the averaged energy. While evaluating the integral in Eq. (31) we hold both y and μ fixed, since they are constants in the unperturbed system. Eliminating t from Eqs. (29) and (30), and using $(\,)'$ for $d(\,)/d\mu$, we obtain

$$\bar{y}' = -2\bar{x} \tag{32}$$

Equation (32) is a single first-order differential equation for the slow trajectories in the μy plane.

Recall that $k = 1$ at the energy levels associated with the saddles and separatrices on the sphere, or equivalently, with the dashed lines in the μy plane. Since $K(1) = \infty$, the method of averaging is not applicable at the separatrix crossings; thus, we expect Eq. (32) to be inaccurate in a neighborhood of the separatrix crossings.

When the roots of the quartic are all real, $x(u; k)$ is given by Eq. (27), and Eq. (31) becomes

$$\bar{x} = \frac{\beta}{K}\left\{K + \frac{\pi(\alpha^2 - \alpha_1^2)\left[1 - \Lambda_0(\psi, k)\right]}{2\sqrt{\alpha^2(1-\alpha^2)(\alpha^2 - k^2)}}\right\} \tag{33}$$

where $\psi = \sin^{-1}\sqrt{(1-\alpha^2)/(1-k^2)}$, and $\Lambda_0(\psi, k)$ is Heuman's lambda function. When two of the roots are complex, $x(u; k)$ is given by Eq. (28), and $\bar{x}$ is given by

$$\bar{x} = \frac{\beta}{\alpha K}\left\{\alpha_1 K + \frac{\alpha - \alpha_1}{1 - \alpha^2}\,\Pi(\hat{\alpha}^2, k)\right\} \tag{34}$$

where $\Pi(\hat{\alpha}^2, k)$ is a complete elliptic integral of the third kind with parameter $\hat{\alpha}^2 = \alpha^2/(\alpha^2 - 1)$. Details regarding the elliptic integrals in Eqs. (33) and (34) may be found in Ref. 19.

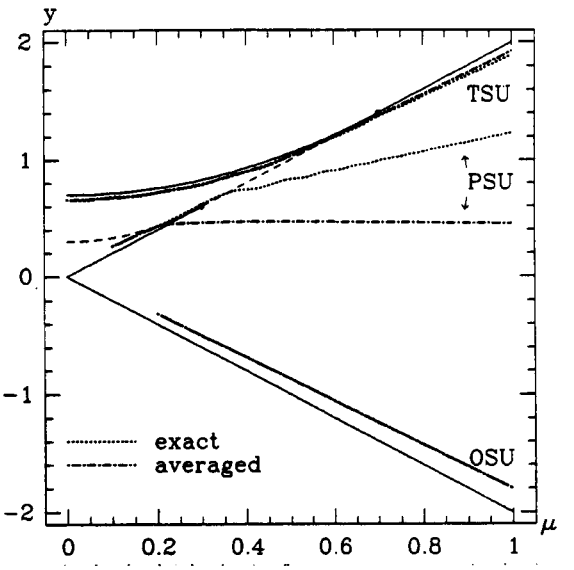

Fig. 7 Comparison of averaged and exact trajectories.

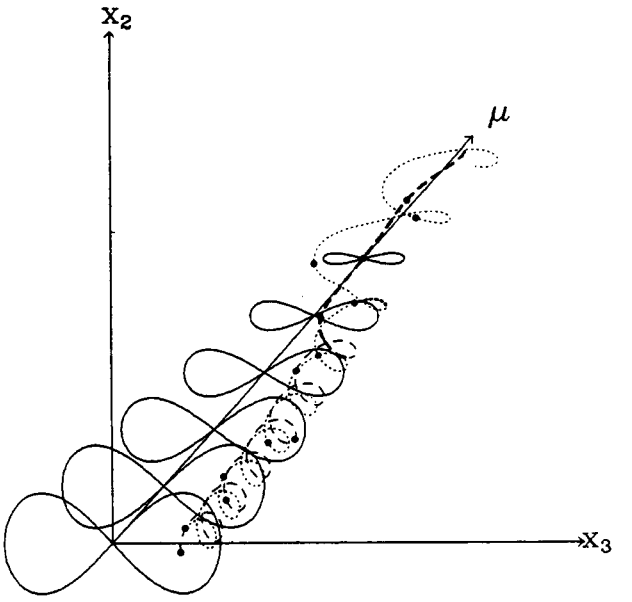

Fig. 8 Two trajectories near an instantaneous separatrix crossing.

Note that since the cone angle (see Fig. 1) is the angle between $\boldsymbol{h}$ and $\hat{\boldsymbol{e}}_1$, it follows that in the dimensionless variables, the cone angle is $\eta = \cos^{-1}x$. For given y and μ the average cone angle is

$$\bar{\eta} = \cos^{-1}\bar{x} \tag{35}$$

Thus Eq. (33) or (34) may be used with Eq. (35) to compute the average cone angle.

Numerical integration of Eq. (32) with initial values of μ and y generates a trajectory in the μy plane, which according to the averaging theorem remains within $\mathcal{O}(\epsilon)$ of the exact solution on a time scale of $\mathcal{O}(1/\epsilon)$. Recall however, that the dashed lines in

the μy plane represent instantaneous separatrices, where the period of the $\epsilon = 0$ solution becomes infinite and averaging is not valid. Although separatrix crossings present no difficulty in numerically integrating Eq. (32), we will see in what follows that the divergence between solutions of the averaged and unaveraged equations is due to this separatrix crossing.

Comparisons and Discussion

In Fig. 7 we compare averaged solutions [Eq. (32)] with "exact" solutions of Eqs. (8–11), for $i_2 = -0.3$, $i_3 = -0.7$, and $\epsilon = 0.01$. For oblate spinup, the two solutions shown in Fig. 7 are indistinguishable. Note that, since oblate spinup trajectories in the μy plane are nearly straight lines, Eq. (32) implies $\bar{x} \approx$ const, and Eq. (35) implies $\bar{\eta} \approx$ const. Thus spinup has little effect on the nutation angle for oblate spacecraft. Transverse and prolate spinup, however, show a notable divergence of the two solutions. For transverse spinup the error is small, but for prolate spinup it can become large. Of course, decreasing ϵ improves the agreement, as shown in Table 1, where the percent relative error is given as $100|(y - \bar{y})/y|$ evaluated at $\mu = 1$ for the three spinup problems and for five values of ϵ.

The reason for the significant error in transverse and prolate spinup is the separatrix crossings discussed in previous sections. The averaged and unaveraged paths begin to diverge when the trajectory reaches the vicinity of the instantaneous separatrix, where the period of the unperturbed oscillation of x becomes infinite and averaging is not applicable.[18] This separatrix crossing is sometimes called passage through resonance, and the region where the unperturbed period becomes infinite is called the resonance manifold.[20] Here the resonance manifold consists of the energy levels associated with the instantaneous separatrices, i.e., the dashed lines in the μy plane.

It is important to note that the error depends on the phase u of a trajectory as it crosses the instantaneous separatrix. Recall that fixing y and μ defines a particular integral curve on the momentum sphere, whereas u determines where a point is on the integral curve. Since the averaged system is independent of initial phase, averaging maps all points on an initial integral curve to a single final integral curve. However, the behavior of trajectories of the unaveraged system may be quite different due to the separatrix crossing. This is illustrated in Fig. 8, where we show two trajectories with initial conditions on the same constant energy curve but with slightly different initial phases. The instantaneous separatrices are superimposed onto the figure to aid in visualization of the separatrix crossing. The two trajectories are represented as dotted and dashed curves, and the large dots on the trajectories indicate where the trajectories pass through the planes of the instantaneous separatrices. It is evident that after the separatrix has "disappeared," the two trajectories are quite different: the dotted trajectory crosses the separatrix far from the saddle point and has a large residual cone angle, whereas the dashed trajectory gets delayed near the saddle and has a smaller residual cone angle. According to a theorem of Neishtadt as found in Ref. 21, the set of initial conditions which get delayed near the saddle has small measure m for small ϵ, i.e., $m = \mathcal{O}(\sqrt{\epsilon})$.

Actually, the averaged equation is quite accurate almost arbitrarily close to the separatrix; the large error is due to the fact that the separatrix crossing is extremely sensitive to the phase. To improve the agreement between Eq. (32) and Eqs. (8–11) for those trajectories that cross a separatrix, one could introduce an equation for the fast variation of u, by applying variation of parameters to Eq. (23), then develop a "separatrix crossing model" valid in an $\mathcal{O}(\epsilon)$ neighborhood of the resonance manifold, taking into account the additional phase information.[16] Such a procedure would yield an accurate description of most trajectories; however, no separatrix crossing model, however accurate, can accurately connect the averaged equations across the separatrix for all initial conditions. This is true because of the combined effects of two phenomena: 1) the method of averaging introduces a small $[\mathcal{O}(\epsilon)]$ error in amplitude and phase and 2) the small $[\mathcal{O}(\sqrt{\epsilon})]$ set of trajectories that get delayed near the saddle point during the separatrix crossing is extremely sensitive to changes in initial phase.

Conclusions

We have shown that the equations of motion for spinup of axial dual-spin spacecraft can be approximately reduced to a single first-order ordinary differential equation which describes the slow variation of energy during spinup of the rotor by a small constant torque. This equation governs the dynamics on the μy plane, the introduction of which simplifies the geometrical depiction of spinup dynamics, which previously required one to picture solutions on a sequence of spheres. Our derivation used conservation of angular momentum and the method of averaging applied to the elliptic function solution of the unperturbed problem. The averaged equation accurately describes spinup dynamics outside a neighborhood of the resonance manifolds, the latter consisting of curves in the μy plane corresponding to separatrices of the unperturbed system. We showed that oblate spinup can be described accurately by the averaged equation since this problem does not require that a trajectory cross the resonance manifolds. The final outcome of transverse spinup can be less accurately predicted by our method, since in this case a resonance manifold, i.e., a separatrix of the $\epsilon = 0$ problem, must be crossed once. In the case of prolate spinup, the motion must pass through a resonance manifold twice, and so the results of using the simplified strategy presented in this paper are in poorer agreement with numerical integration of the exact equations.

References

[1]Cochran, J. E., Shu, P.-H., and Rew, S. D., "Attitude Motion of Asymmetric Dual-Spin Spacecraft," *Journal of Guidance, Control, and Dynamics*, Vol. 5, No. 1, 1982, pp. 37–42.

[2]Gebman, J. R., and Mingori, D. L., "Perturbation Solution for the Flat Spin Recovery of a Dual-Spin Spacecraft," *AIAA Journal*, Vol. 14, No. 7, 1976, pp. 859–867.

[3]Hubert, C. H., "Dynamics of the Generalized Dual-Spin Turn," *RCA Review*, Vol. 41, No. 3, 1980, pp. 449–471.

[4]Hubert, C. H., "Spacecraft Attitude Acquisition from an Arbitrary Spinning or Tumbling State," *Journal of Guidance and Control*, Vol. 4, No. 2, 1981, pp. 164–170.

[5]Junkins, J. L., and Turner, J. D., *Optimal Spacecraft Rotational Maneuvers*, Elsevier Science, Amsterdam, The Netherlands, 1986, pp. 119–127.

[6]Guelman, M., "On Gyrostat Dynamics and Recovery," *Journal of the Astronautical Sciences*, Vol. 37, No. 2, 1989, pp. 109–119.

[7]Scher, M. P., and Farrenkopf, R. L., "Dynamic Trap States of Dual-Spin Spacecraft," *AIAA Journal*, Vol. 12, No. 12, 1974, pp. 1721–1725.

[8]Cochran, J. E., "Nonlinear Resonances in the Attitude Motion of Dual-Spin Spacecraft," *Journal of Spacecraft and Rockets*, Vol. 14, No. 9, 1977, pp. 562–572.

[9]Cochran, J. E., and Beaty, J. R., "Near-Resonant and Transition Attitude Motion of a Class of Dual-Spin Spacecraft," *Journal of the Astronautical Sciences*, Vol. 26, No. 1, 1978, pp. 19–45.

[10]Kinsey, R. J., Mingori, D. L., and Rand, R. H., "Spinup Through Resonance of Rotating Unbalanced Systems with Limited Torque," *Proceedings of the 1990 AIAA/AAS Astrodynamics Conference* (Portland, OR), Pt. 2, AIAA, Washington, DC, Aug. 1990, pp. 805–813.

[11]Or, A. C., "Resonances in the Despin Dynamics of Dual-Spin Spacecraft," *Journal of Guidance, Control, and Dynamics*, Vol. 14, No. 2, 1991, pp. 321–329.

[12]Rand, R. H., Kinsey, R. J., and Mingori, D. L., "Dynamics of Spinup through Resonance," *International Journal of Nonlinear Mechanics*, Vol. 27, No. 3, 1992, pp. 489–502.

[13]Hughes, P. C., *Spacecraft Attitude Dynamics*, Wiley, New York, 1986, Chaps. 3 and 6.

[14]Hall, C. D., "Equivalence of Two Classes of Dual-Spin Spacecraft Spinup Problems," *Journal of Guidance, Control, and Dynamics*, Vol. 15, No. 4, 1992, pp. 1032–1034.

[15]Hall, C. D., and Rand, R. H., "Spinup Dynamics of Axial Dual-

Spin Spacecraft," *Astrodynamics 91*, Vol. 76, Advances in the Astronautical Sciences, Univelt Inc., San Diego, CA, 1992, pp. 641–660.

[16]Hall, C. D., *An Investigation of Spinup Dynamics of Axial Gyrostats Using Elliptic Integrals and the Method of Averaging*, Ph.D. Thesis, Dept. of Theoretical and Applied Mechanics, Cornell Univ., Ithaca, NY, 1992.

[17]Guckenheimer, J., and Holmes, P., *Nonlinear Oscillations, Dynamical Systems, and Bifurcations of Vector Fields*, Springer-Verlag, New York, 1983, pp. 149, 150.

[18]Coppola, V. T., and Rand, R. H., "Chaos in a System with a Periodically Disappearing Separatrix," *Nonlinear Dynamics*, Vol. 1, 1990, pp. 401–420.

[19]Byrd, P. F., and Friedman, M. D., *Handbook of Elliptic Integrals for Engineers and Scientists*, Springer-Verlag, Berlin, 2nd ed., 1971.

[20]Sanders, J. A., and Verhulst, F., *Averaging Methods in Nonlinear Dynamical Systems*, Springer-Verlag, New York, 1985, Chaps. 3 and 5.

[21]Lochak, P., and Meunier, C., *Multiphase Averaging for Classical Systems: With Applications to Adiabatic Theorems*, Springer-Verlag, New York, 1988, Chaps. 1–4.